AD-A047 298 DEFENCE RESEARCH ESTABLISHMENT PACIFIC VICTORIA (BRIT--ETC F/G 20/1
THE REFLECTION OF ACOUSTIC WAVES IN SEA WATER FROM AN ICE COVER--ETC(U)
JUN 77 R VERRALL, J GANTON

UNCLASSIFIED DREP-TM-77-8 NL

| OF |
AD
A047 298

END
DATE
FILMED
1 - 78
DDC

DEFENCE RESEARCH ESTABLISHMENT PACIFIC

VICTORIA, B.C.

This information is furnished with the express understanding that proprietary and patent rights will be protected.

(9) Technical Memorandum 77-8

(14) DREP-TM-77-8

(6) THE REFLECTION OF ACOUSTIC WAVES IN SEA WATER FROM AN ICE COVERED SURFACE.

(10) R. Verrall and J. Ganton

(11) June 1977 (12) 31p.

Approved for distribution J T Hunn

RESEARCH AND DEVELOPMENT BRANCH

DEPARTMENT OF NATIONAL DEFENCE

CANADA

DISTRIBUTION STATEMENT A
Approved for public release;
Distribution Unlimited

AD A03 246

1B

ABSTRACT

Measurements of the acoustic reflectivity of the lower surface of sea ice were made at several location in the channels of the Canadian Arctic Archipelago from 1971 to 1973. The distance between the projector and hydrophone was typically 100 to 300 m; the grazing angle at the ice-water interface ranged up to 30 deg, and the frequency limits were 200 Hz and 20,000 Hz. The measured reflectivities, which are presented here, show large excursions from unity. Reflectivities of -15 dB are not uncommon in spite of the uniform flatness of the ice-water interface and in spite of the shallowness of the grazing angle. However, a calculation based on Kirchhoff's Integral Theorem and involving an integration over the interface indicates that the observed undulation in the ice-water interface is sufficient to account for the observed results.

ACCESSION for
NTIS White Section ✓
DDC Buff Section ☐
UNANNOUNCED ☐
JUSTIFICATION
BY
DISTRIBUTION/AVAILABILITY CODES
Dist. AVAIL. and/or SPECIAL
A

INTRODUCTION

The problem of understanding and predicting the propagation of sound in the ice-covered seas of the Arctic requires a knowledge of the behaviour of sound waves as they reflect from the water-ice boundary. The scattering or reflection of sound from the rough wave-covered surface of more southern oceans has been fairly extensively studied by (to name a few) Liebermann (1948), Eckart (1953), Marsh, Schulkin and Kneale (1961), Marsh (1963), Ferris and Kuperman (1970). Fortuin (1970) has prepared a survey of the pertinent literature. In the Arctic seas, however, propagation studies have not included the detailed study of the reflection of sound from the under surface of the sea ice.

During springtime field trips in 1971, 1972, and 1973, short range measurements were made of the reflection loss of acoustic waves under the surface of the sheet of ice upon which the camp was situated. Although the ice surface, and therefore presumably the under-ice surface, was always quite smooth, the reflection losses were strongly frequency dependent and as great as 25 dB in some instances.

This report describes the experiment and presents the measured reflectivities. Also, a model based on Kirchhoff's Integral Theorem is developed to explain the large variations that were observed.

LOCATIONS

Measurements were made in April 1971 and April 1972 in Robeson Channel and in May 1972 and April 1973 in Barrow Strait at the locations shown in Figure 1. The ice on which the camp was located was, in all cases, smooth, first-year ice having a thickness of 1.8 m in 1971 and 1972 and 2.4 m in 1973. Figure 2 is a photograph showing the snow-covered ice surface in the neighbourhood of the camp in Barrow Strait. In 1973, with the aid of Canadian Forces divers, the undulations of the ice-water interface were mapped with a grid spacing of 1 meter over an area in the region of the camp measuring 8 by 31 meters. Figure 3 is a photograph of the underside of the ice surface and Figure 4 is an isometric diagram of the mapped surface. The R.M.S. variation of the level of this interface was only 2 cm and the subjective impression of the divers was that the interface was remarkably smooth.

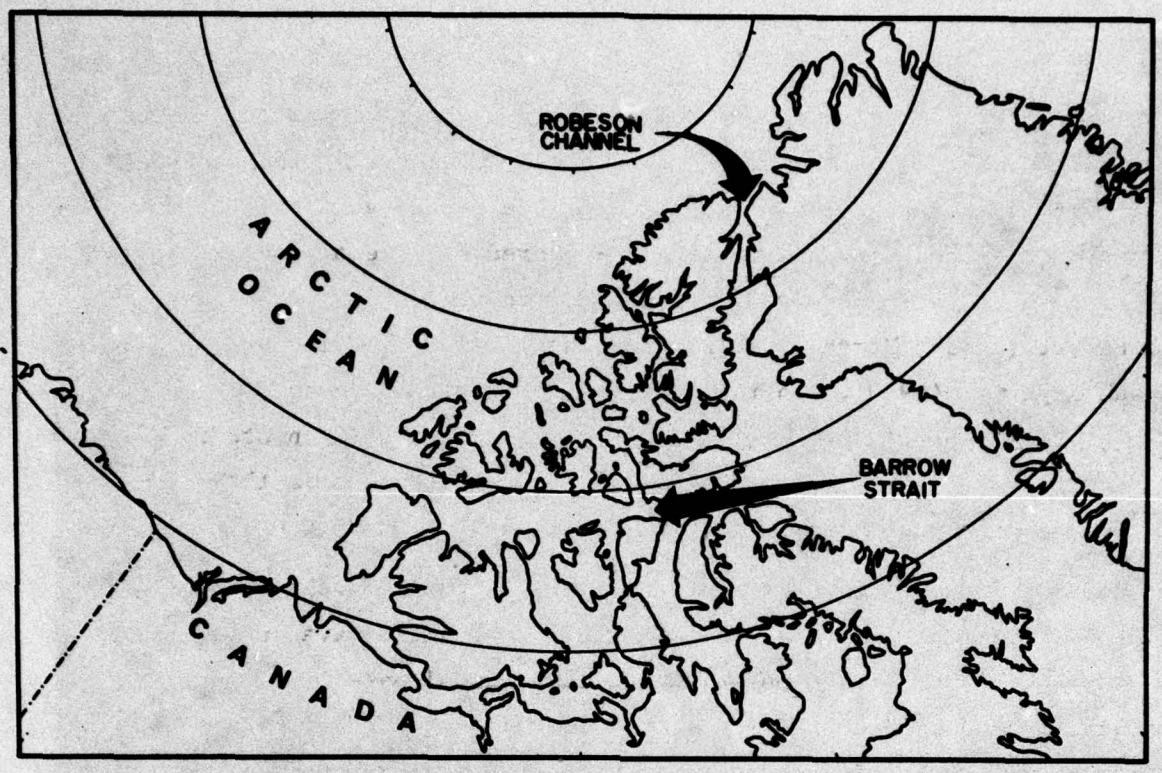

Figure 1. Map of the Arctic Islands showing the areas where reflectivity experiments were performed.

Figure 2. Photograph of an ice-camp illustrating the smoothness of the ice

Figure 3. A photograph of the underside of the ice surface illustrating the smoothness of the interface. Projecting into the water and giving a feeling for the scale of the picture is a bamboo pole and flag. The bubbles at the surface are the divers' exhaust air.

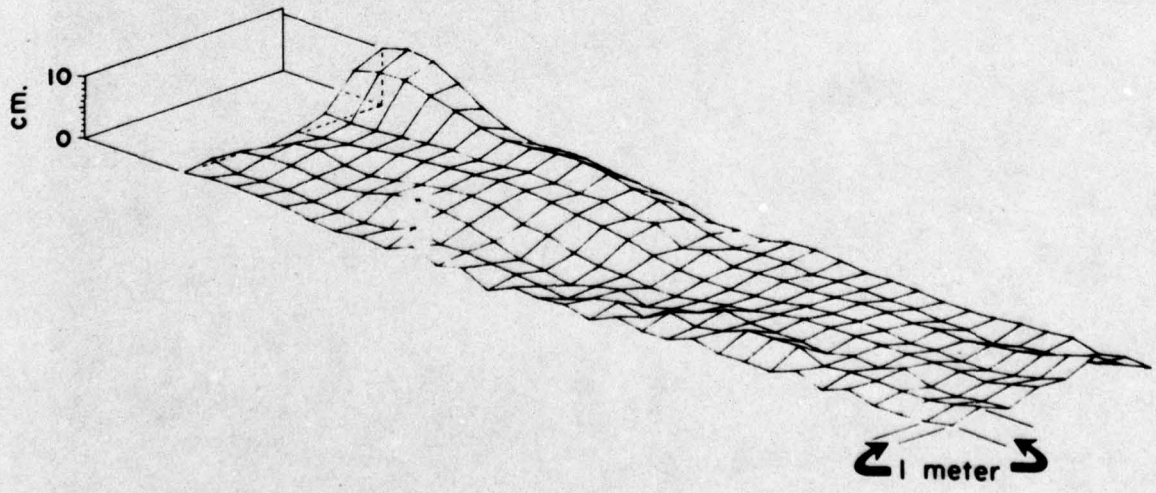

Figure 4. Isometric diagram of the ice-water interface measured in 1973 in Barrow Strait.

DESCRIPTION OF EXPERIMENT

The measurement of the sound reflectivity consisted of a comparison of the amplitude of a c.w. sound pulse which had travelled in a direct path from projector to hydrophone with the magnitude of the same pulse which had been returned from the ice-water interface. The geometry of the experiment is indicated in Figure 5. A hydrophone and a projector were lowered to depths d_1 and d_2 through holes in the ice separated by a distance L. In practice the distance L was either 100 meters or 300 meters.

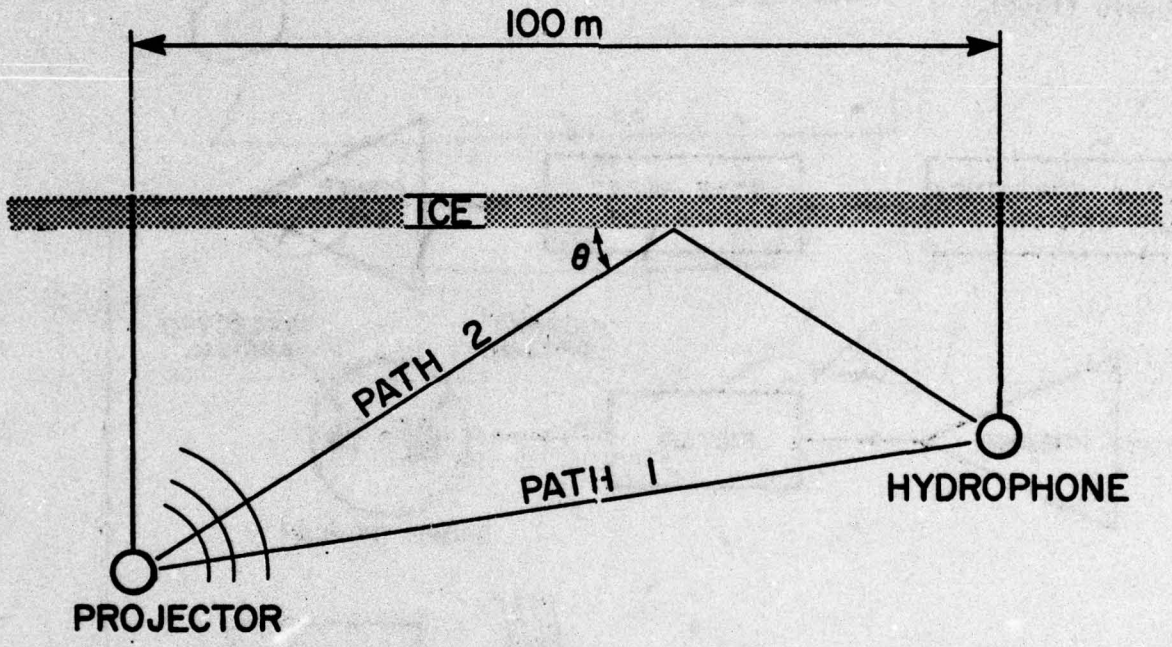

Figure 5. A sketch of the geometry of the experiment.

The distances L, d_1 and d_2 were sufficiently small that the curvature of ray paths was negligible in all calculations. The grazing angle θ in Figure 5 is given by : $\tan\theta = \frac{d_1+d_2}{L}$, and the acoustic travel-time difference between the two paths is easily calculated from the geometry. A typical value of the time difference (L = 100 m, d_1 = 10 m, d_2 = 50 m) is 6 msec. It is this time difference that makes it possible to separate the two travel paths.

The projector was driven by a short constant-frequency tone burst. With reference to the block diagram in Figure 6, the sequence of events was as follows. A variable frequency oscillator was gated by a tone burst generator

which passed a pre-set number of cycles. This burst was amplified and transmitted to the projector. The resulting acoustic signal was detected by the hydrophone, amplified, filtered to improve the signal to noise ratio, and displayed on the oscilloscope. This sequence was repeated every few seconds. The signal was recorded by photographing the oscilloscope face with a Polaroid camera. This technique is similar to that used by Ferris and Kuperman (1970) and Medwin (1966).

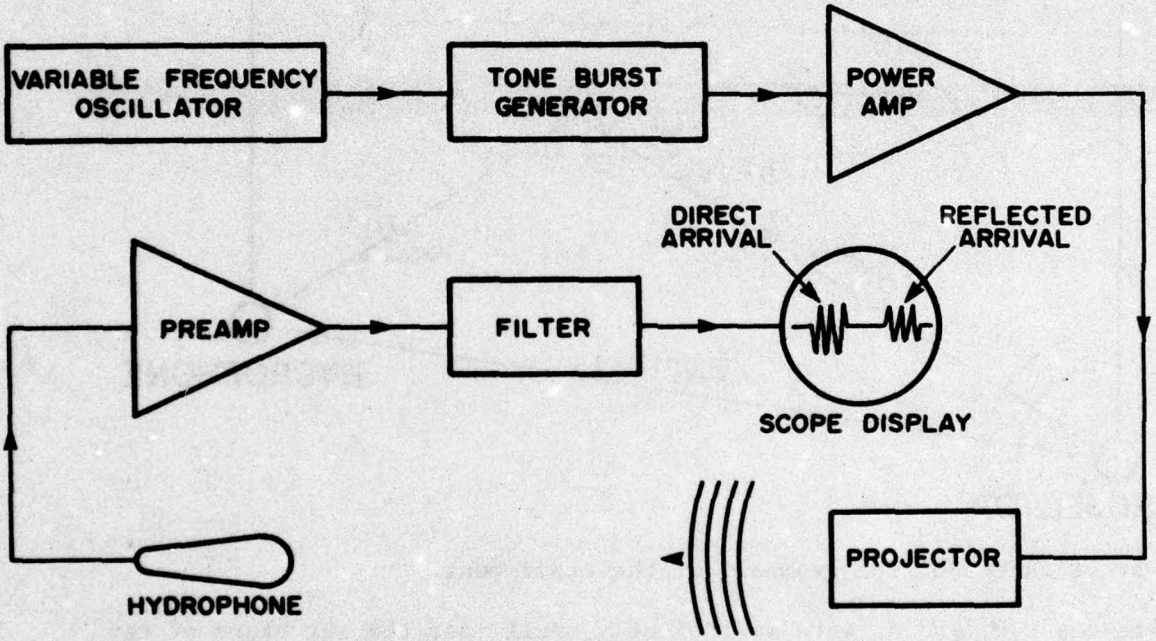

Figure 6. Block diagram of the electronics.

The example photograph in Figure 7 shows the time separation of the signals from the two paths, This time separation sets a lower limit to the frequency that can be used in the experiment since the period for one cycle must be substantially less than the time delay in order to obtain a reliable measurement. In order to make measurements at lower frequencies, the separation of the hydrophone and projector must be increased to increase the time

delay. This increased separation unfortunately reduces the signal to ambient noise ratio because of the limited output power of the projector.

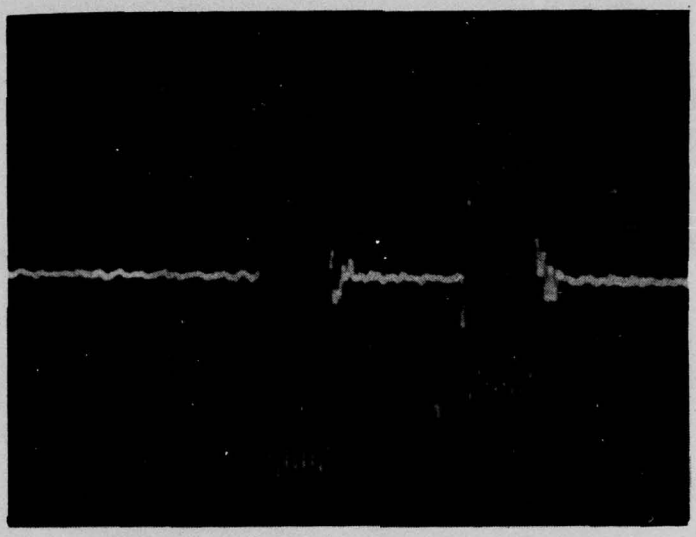

Figure 7. An example photograph of the oscilloscope face showing the direct arrival and the (smaller) reflected arrival.

Three different projectors were used; a Dyna-Empire model J-9 was used at a spacing of 100 m for measurements at higher acoustic frequencies, and a more powerful Marine Resources J-11 or J-13 projector was used at a spacing of 300 m for the lower frequency measurements.

The reflection coefficient was obtained by calculating the ratio of the amplitudes of the reflected pulse and the direct pulse. Since a ratio of two amplitudes is all that was measured, no absolute calibration of the equipment was necessary.

The difference in the direct and reflected path lengths, however, necessitated the use of a small correction to compensate for the different amounts of spherical spreading. Also, at higher frequencies, the increased directivity of the projectors required the application of a correction which,

in the worst case, was less than 1 dB. This correction was made by assuming that the radiation pattern of the projector was that of a simple circular piston. The far field (amplitude) radiation pattern (normalized to 1 at $\theta = 0$) for a piston is given by (Urick, 1967)

$$D(\theta,\lambda) = \frac{2J_1(\frac{2\pi}{\lambda} a \sin\theta)}{\frac{2\pi}{\lambda} a \sin\theta}$$

where the direction θ is measured with respect to the normal to the active surface of the projector,

a is the radius of piston (2.85 cm in the case of the J-9 and 5.1 cm in the case of the J-11 and J-13)

λ is the wavelength, and

J_1 is the first order Bessel function of the first kind.

The angle θ was calculated from the geometry of the experiment and the orientation of the projector. The J-9, when used, was oriented to point horizontally in the direction of the hydrophone; the J-11 and the J-13, on the other hand, were suspended to point vertically upward.

RESULTS

Figure 8 through 11 show the corrected reflectivity in decibels as a function of frequency. Each of the figures shows all the measurements at one location. Each diagram indicates the horizontal separation and depths of the projector and hydrophone, the grazing angle θ, and the type of projector. One of the most noticeable features of the plots is the overall low reflectivity; values of -5dB to -10dB are common. The other remarkable property is the large variation of reflectivity with frequency; sharp minima are often present. There are also some examples showing the reflectivity to be greater than 0 dB suggesting interference phenomena.

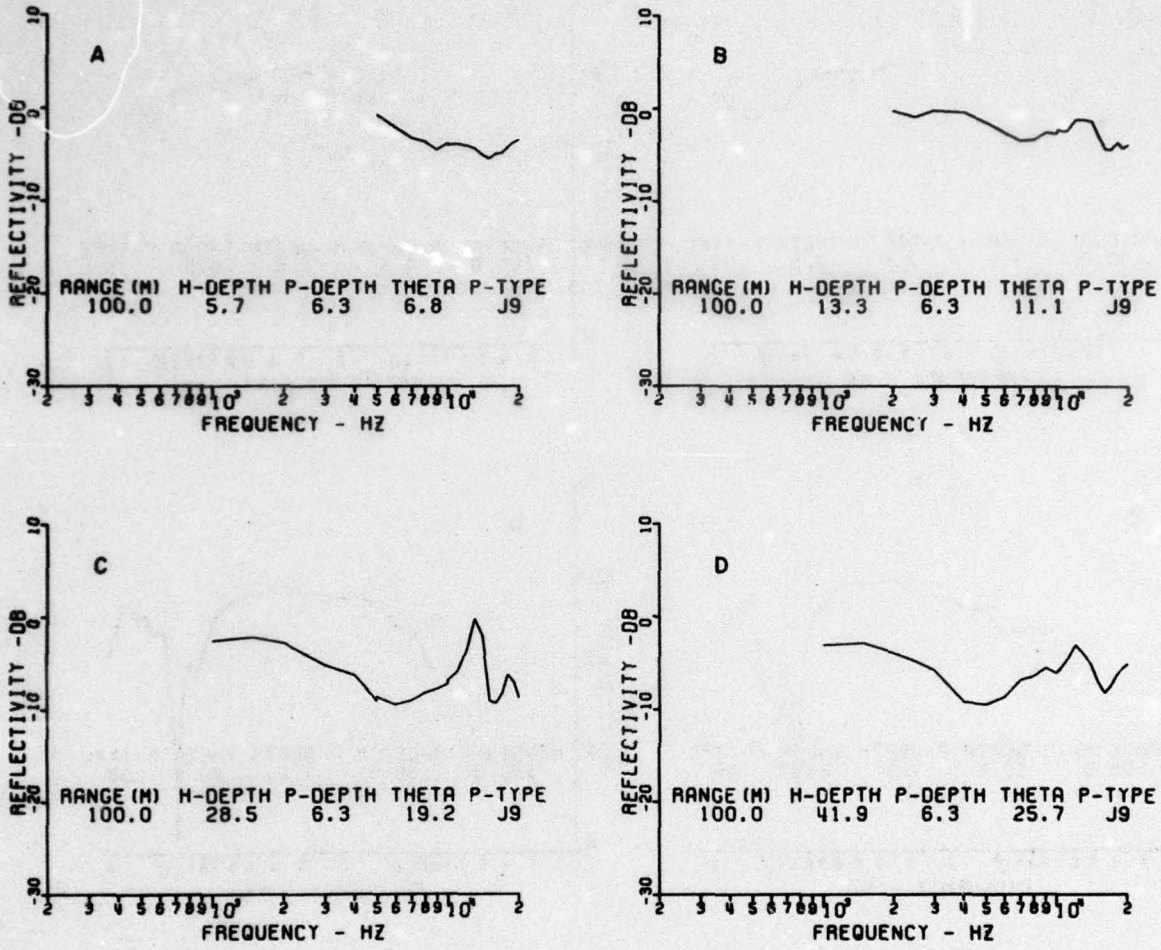

Figure 8. Reflectivity measured in Robeson Channel in April, 1971.

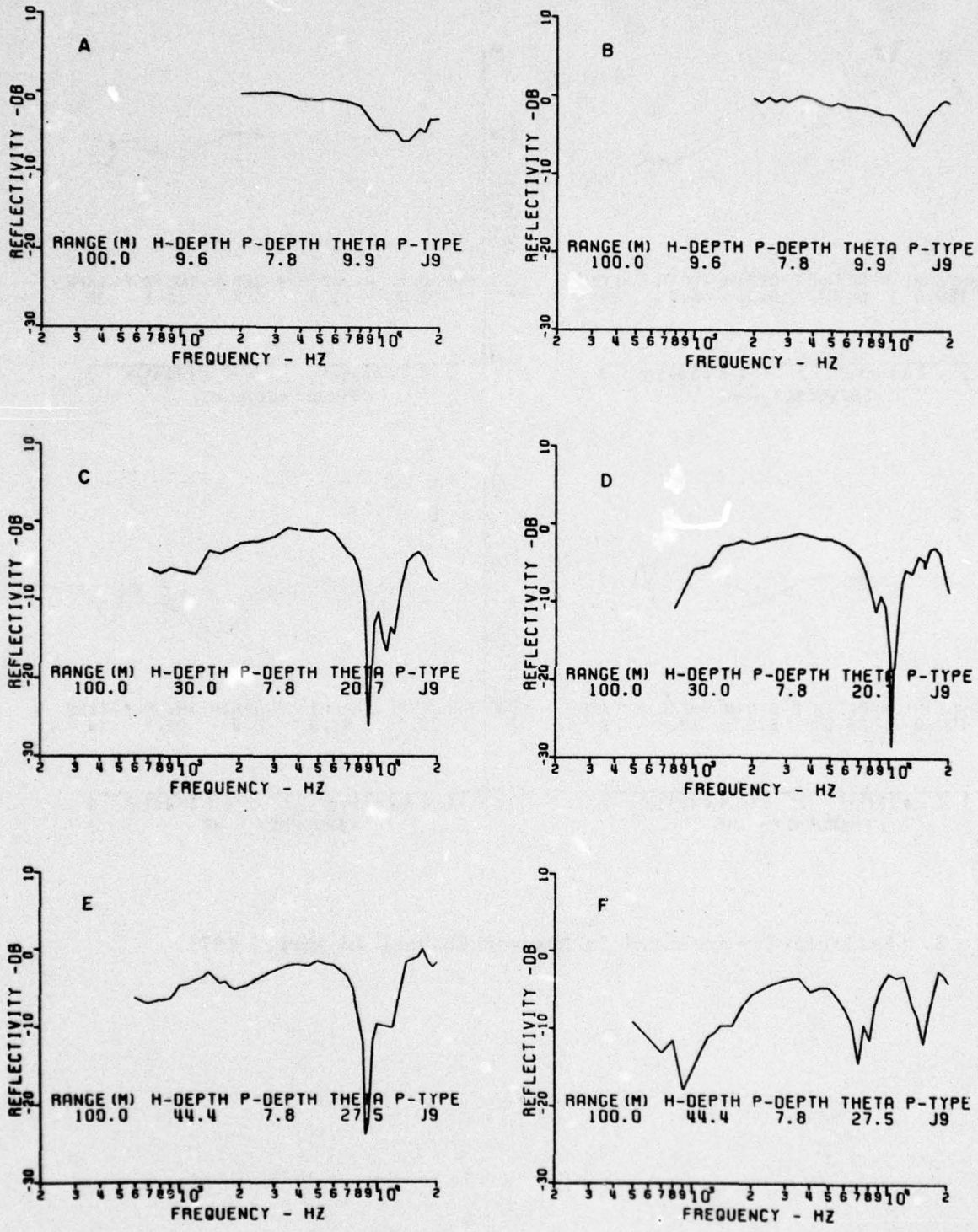

Figure 9. Reflectivity measured in Robeson Channel in April, 1972.

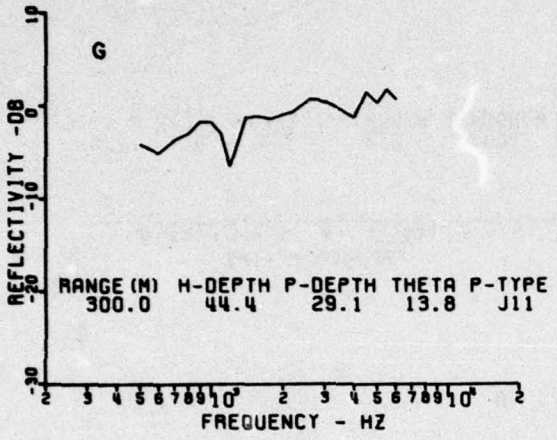

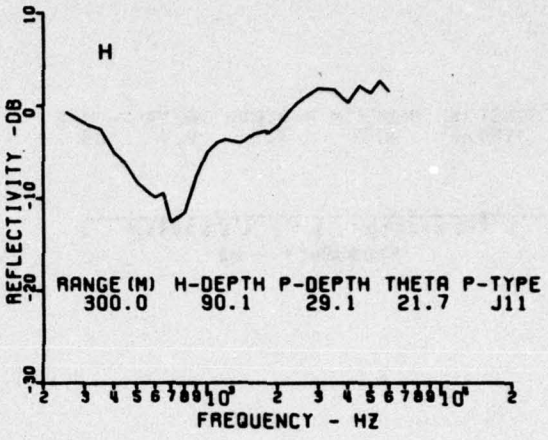

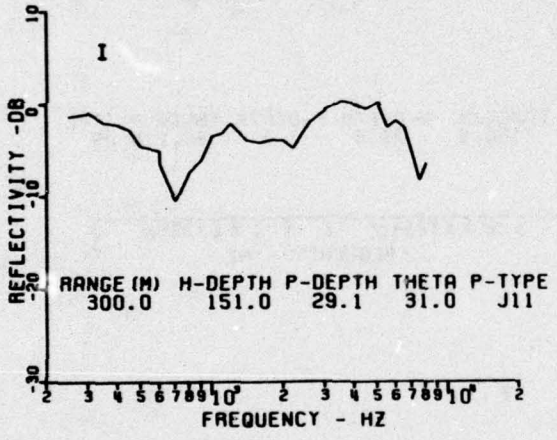

Figure 9. Continued.

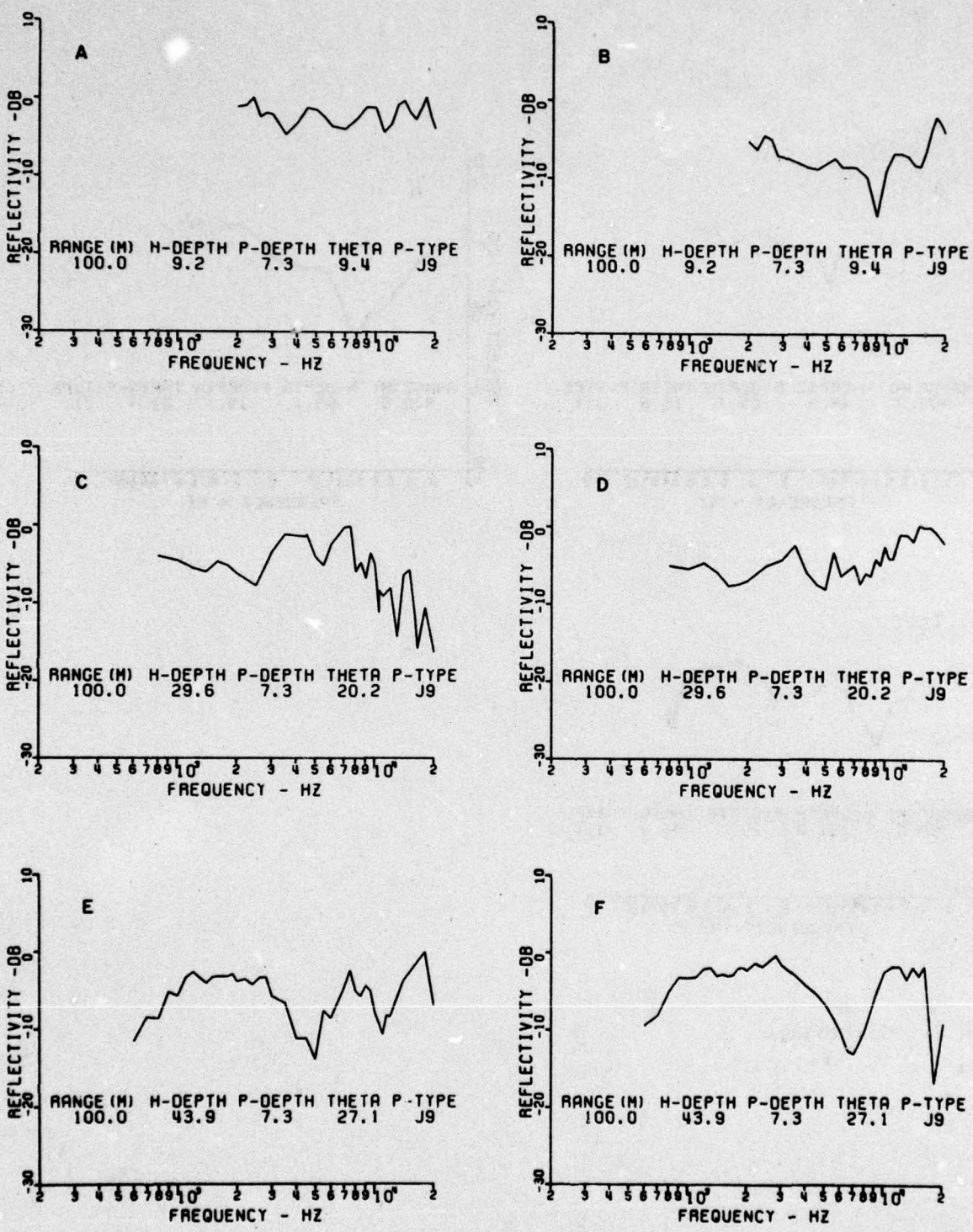

Figure 10. Reflectivity measured in Barrow Strait in April, 1972.

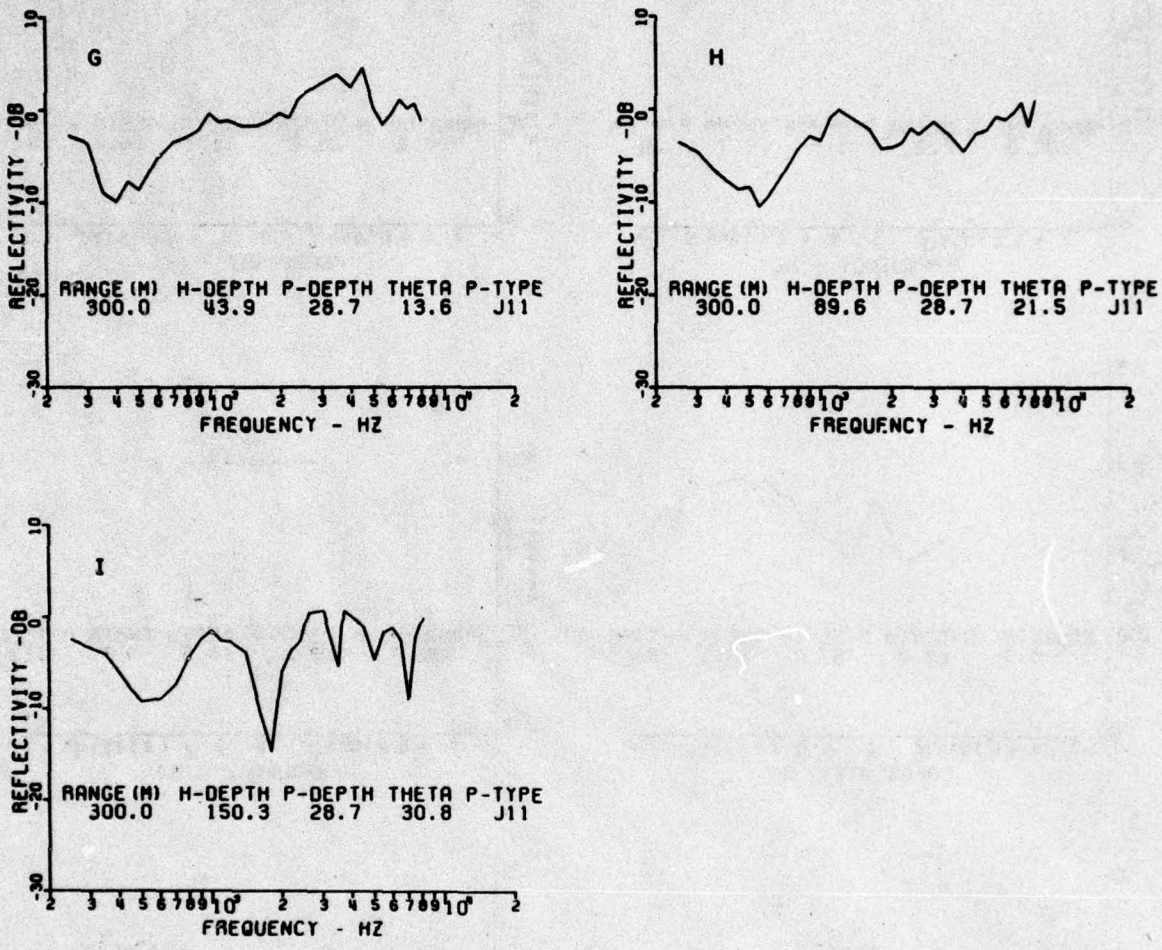

Figure 10. Continued.

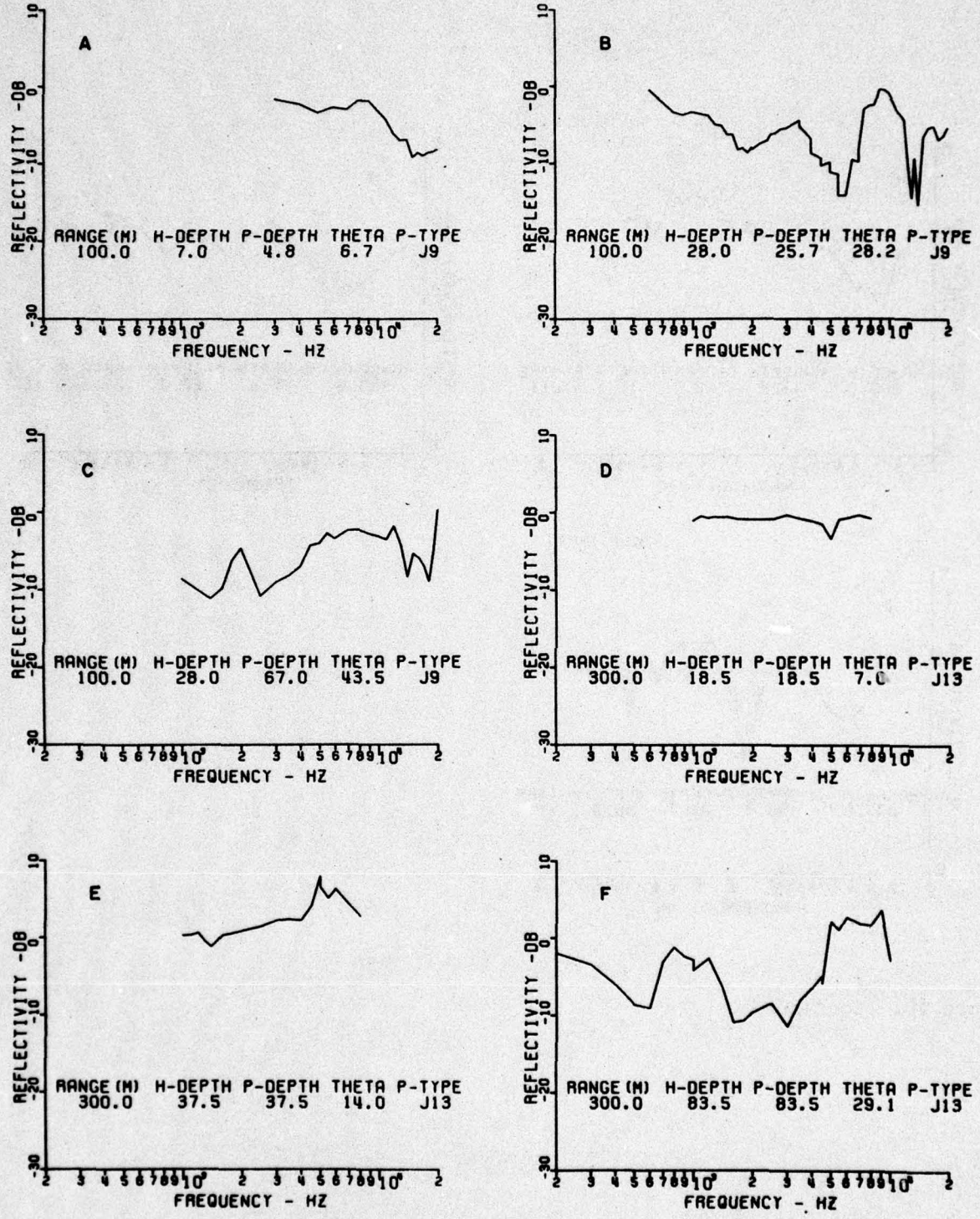

Figure 11. Reflectivity measured in Barrow Strait in April, 1973.

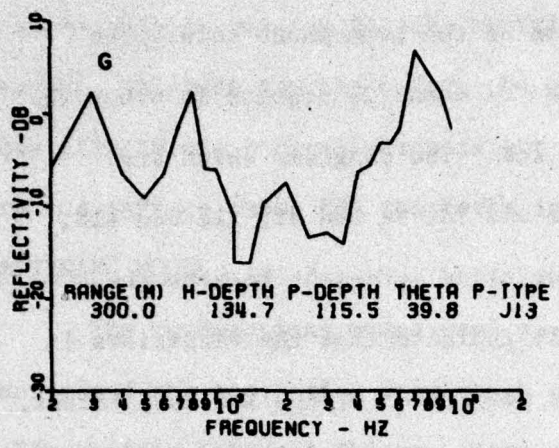

Figure 11. Continued.

Some of the diagrams occur in pairs in which all the listed parameters are the same. The difference is the location of the hydrophone hole. The two holes were separated by an azimuth angle of about 20 degrees in order to reflect the sound from different samples of ice. The diagrams which are paired in this way are Figures 9a and 9b, 9c and 9d, 9e and 9f, 11a and 11b, 11c and 11d, and 11e and 11f. The lack of detailed agreement between the diagram pairs, expecially those in Figure 11, indicate that the variations in reflectivity are not mainly due to the gross properties of the ice but, rather, are due to the change of some property which varies rapidly with location. The roughness of the ice-water interface is an obvious possibility.

Another interesting feature which suggests an interference phenomenon is illustrated in the photograph shown in Figure 12.

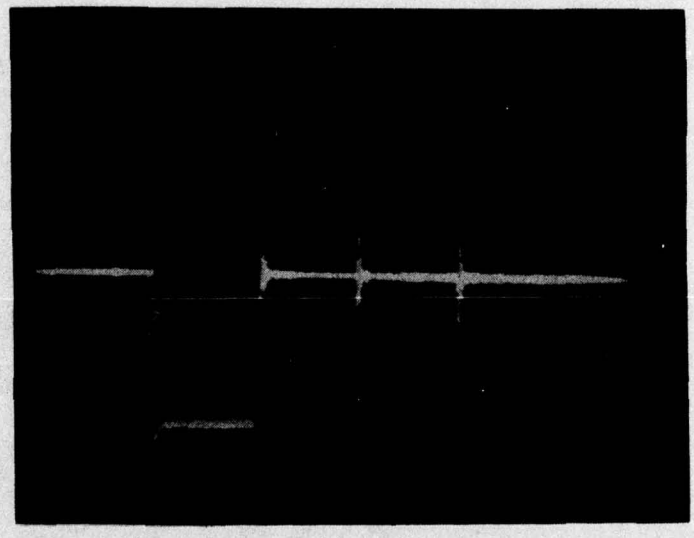

Figure 12. This photograph shows the interference effect at the beginning and end of the reflected pulses. This effect is prominent at frequencies where the reflectivity is very low.

This picture, which was taken near a reflectivity minimum shows the reflected pulse sharply decreasing in size shortly after onset and then increasing to the original amplitude shortly before the end of the pulse. As will be shown, these effects are generally consistent with the scattering of sound from a hard ice surface whose RMS roughness is only a few centimeters.

SCATTERING MODEL

The mathematical model used to establish the connection between our results and the scattering from rough surfaces is, in essence, an application of Kirchhoff's Integral Theorem (Born and Wolf, 1959). This approach to scattering problems is discussed by Beckermann and Spizzichino (1963). The following simplifying assumptions were made, The ice surface is assmed to be rigid. This implies that the local wave reflection is 100% and the reflected wave has a phase shift of zero. The random height variation of the scattering surface was assumed to depend on only one horizontal variable (x). This approximation greatly speeds up the numerical integration over the scattering surface since the integration over the other horizontal variable (y) may be performed analytically by a stationary phase approximation. The effect of these assumptions will be to change only the details of the reflected energy's dependence on frequency; the main effects will be preserved.

The Kirchhoff Integral Theorem states that the amplitude ψ at position P is equal to an integral over the reflecting surface. It is shown in Appendix A that for the approximations assumed here, the amplitude ψ is given by

$$\psi(P) = d_2\sqrt{\frac{k}{2\pi}}\, e^{\frac{-\pi i}{4}} \int \frac{e^{ik(r+s)}}{(r+s)rs^3}\, dx \qquad (1)$$

where $k = \frac{2\pi f}{c}$ with f being the frequency and c the speed of sound

$r = \sqrt{x^2+(d_1+z)^2}$ the distance from the projector to the element of area.

$s = \sqrt{(L-x^2)+(d_2+z)^2}$ the distance from the hydrophone to the element of area.

d_1 = the depth of the projector

d_2 = the depth of the hydrophone

z = the height of the element of area above the mean ice surface

L = the horizontal separation of the projector and hydrophone.

As verification, this integral is evaluated in the Appendix for the case of a flat surface in which $z(x) = 0$ for all x. A stationary phase approximation for this integral yields

$$\psi(P) = \frac{e^{ik(r_o+s_o)}}{r_o+s_o} \qquad (2)$$

where r_o and s_o are the values of r and s corresponding to the point of geometric reflection. This expression is what one would expect of a perfectly reflecting hard surface. As a further check, numerical integrations yield values which agree well both in magnitude and phase with the above expression.

The remaining problem before the integral can be evaluated is to simulate the rough ice-water boundary with a random surface $z(x)$ which has a known correlation function or, equivalently, a known power spectrum. To calculate this spectrum, a series of complex Fourier coefficients of pre-assigned magnitudes but of random phases was generated by a computer and then the inverse Fast Fourier Transform was taken to provide the random surface $z(x)$. The mean-square value of $z(x)$ is easily adjusted and was used as one of the parameters of the surface. The types of spatial

power spectra that were tried were: "White" with a high frequency cut-off, $1/f$, and $1/f^2$ (where f denotes the spatial frequency $1/\lambda$). Figure 13, 14 and 15 show examples of reflectivity for these three types of random surface, the reflection geometry being the same and the RMS value of each surface being 2 cm. It can be seen that these curves, especially Figure 14, resemble the experimental curves in general form. This agreement strongly suggests, that the observed reflection loss was primarily the result of scattering from the rough surface.

Using the ideas developed for this model, it is possible to explain the cancellation phenomenon that was illustrated in Figure 12. Simply expressed, the explanation for these features is that the "Huygen" wavelets which arrive first at the hydrophone come from the area of minimum travel time, the region about the point of geometrical reflection. These wavelets produce a large signal in the hydrophone. Later arriving wavelets fortuitously have the appropriate amplitude and phase to cancel this almost completely. At the end of the pulse, these latter wavelets are not cancelled by the initial ones and the signal becomes large again. A calculation of the reflected pulse was made using a formalism similar to that previously described except that the Green's Function was now time-dependent. A calculated plot of the initial portion of the pulse is shown in Figure 16. As can be seen, the amplitude decreases as the contribution from a wider and wider area of the surface is felt.

An aspect of the problem which is not explained by this model, however, is that the observed reflectivity is nearly always less than 0 dB, whereas the calculated reflectivities are often positive. This implies that some of the energy is being absorbed via a mechanism not included in the model. This could, for example, be the absorption of sound by the porous layer at the water-ice interface.

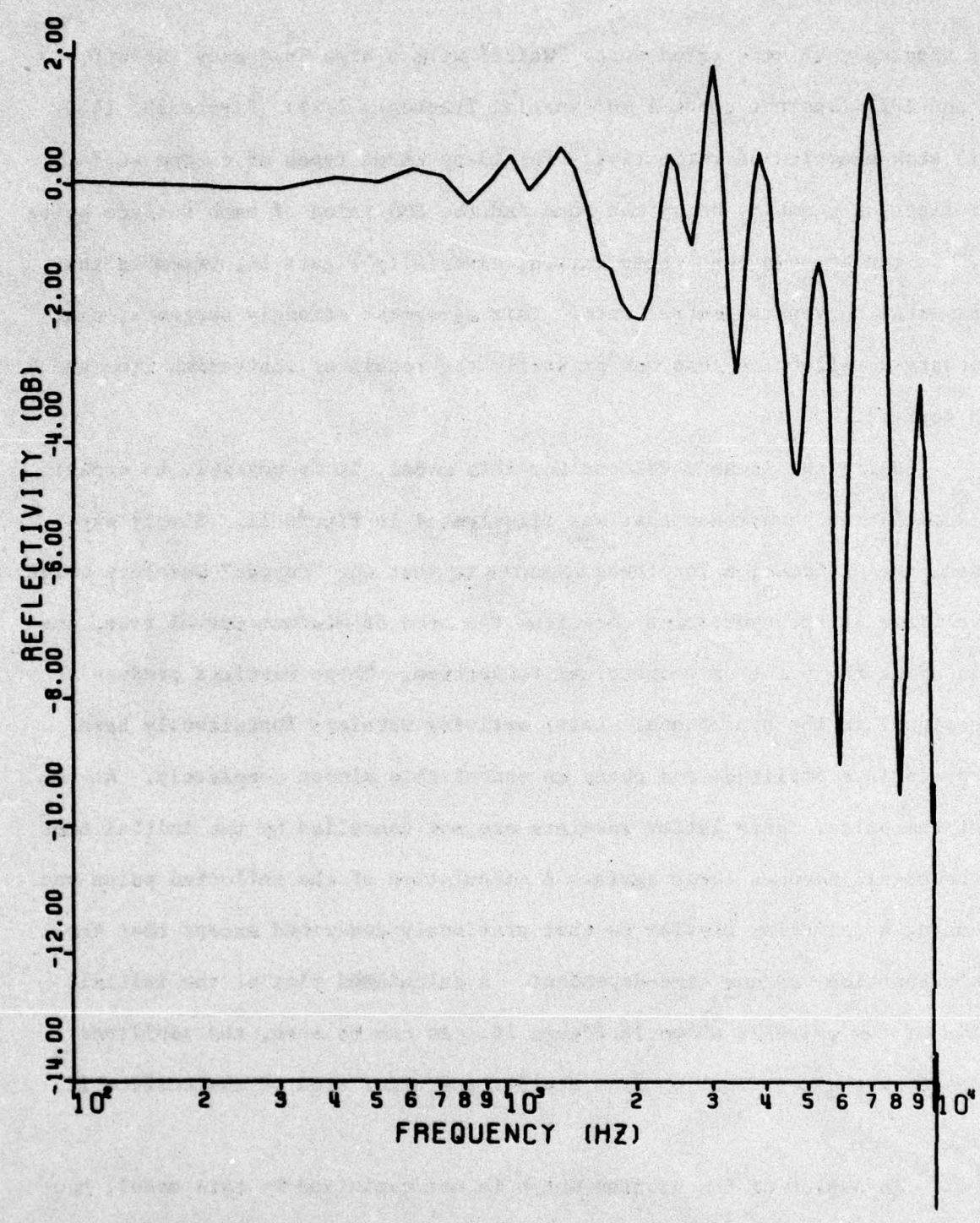

Figure 13. An example of the reflectivity calculated for a random surface whose RMS roughness is 2 cm and whose spatial power spectra is flat.

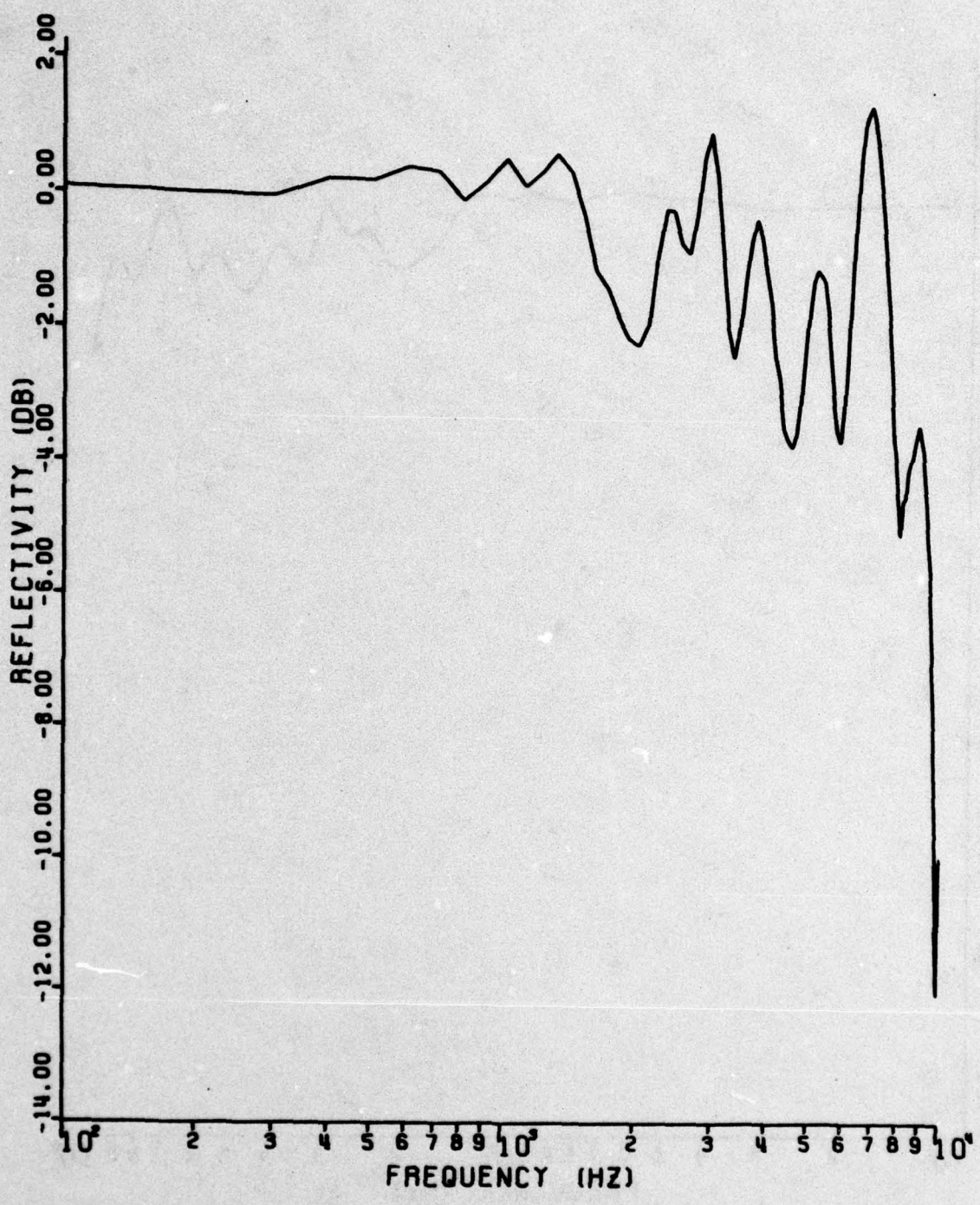

Figure 14. An example of the reflectivity calculated for a random surface whose RMS roughness is 2 cm and whose spatial power spectra goes as 1/wavenumber.

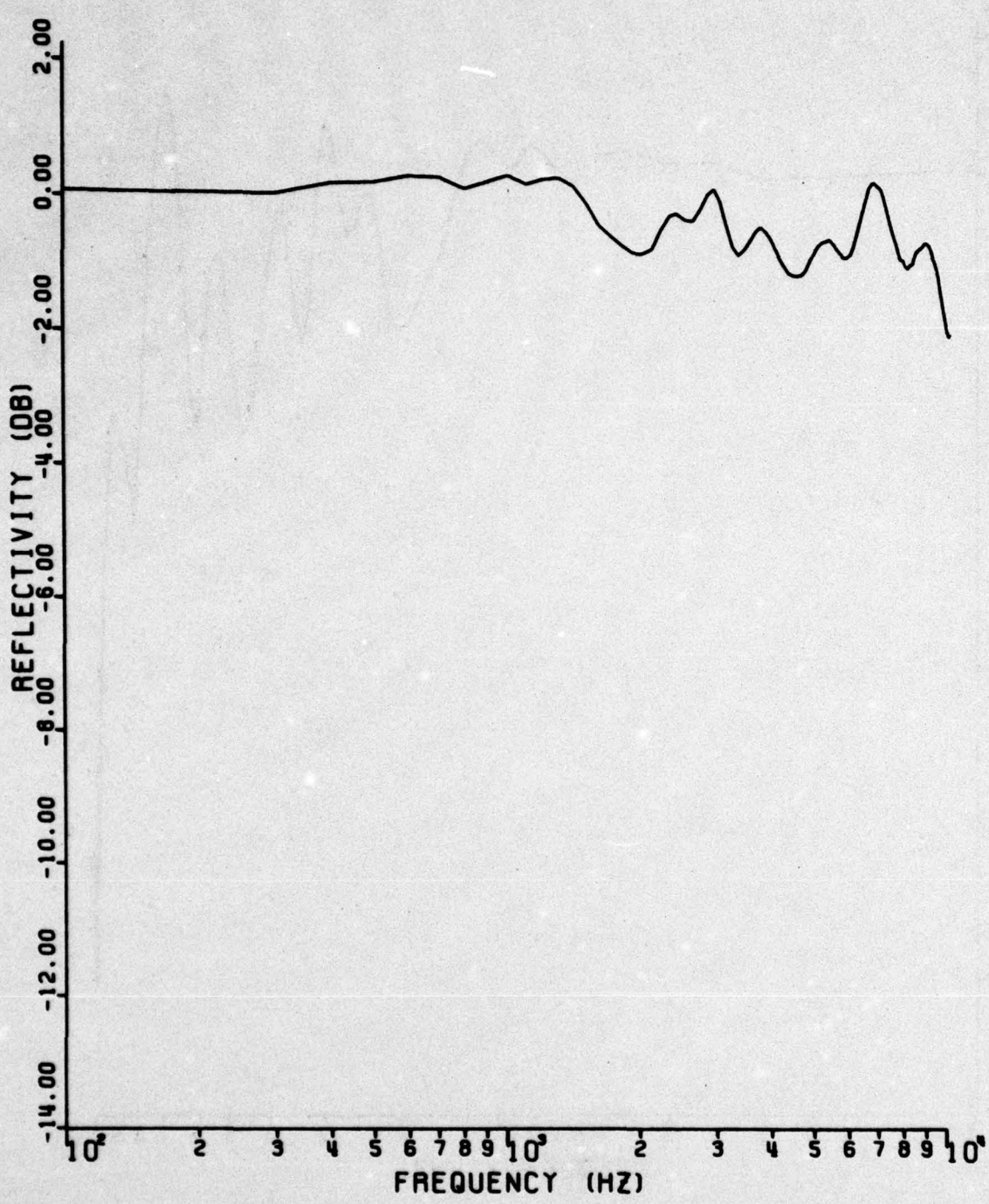

Figure 15. An example of the reflectivity calculated for a random surface whose RMS roughness is 2 cm and whose spatial power spectra goes as 1/wavenumber^2.

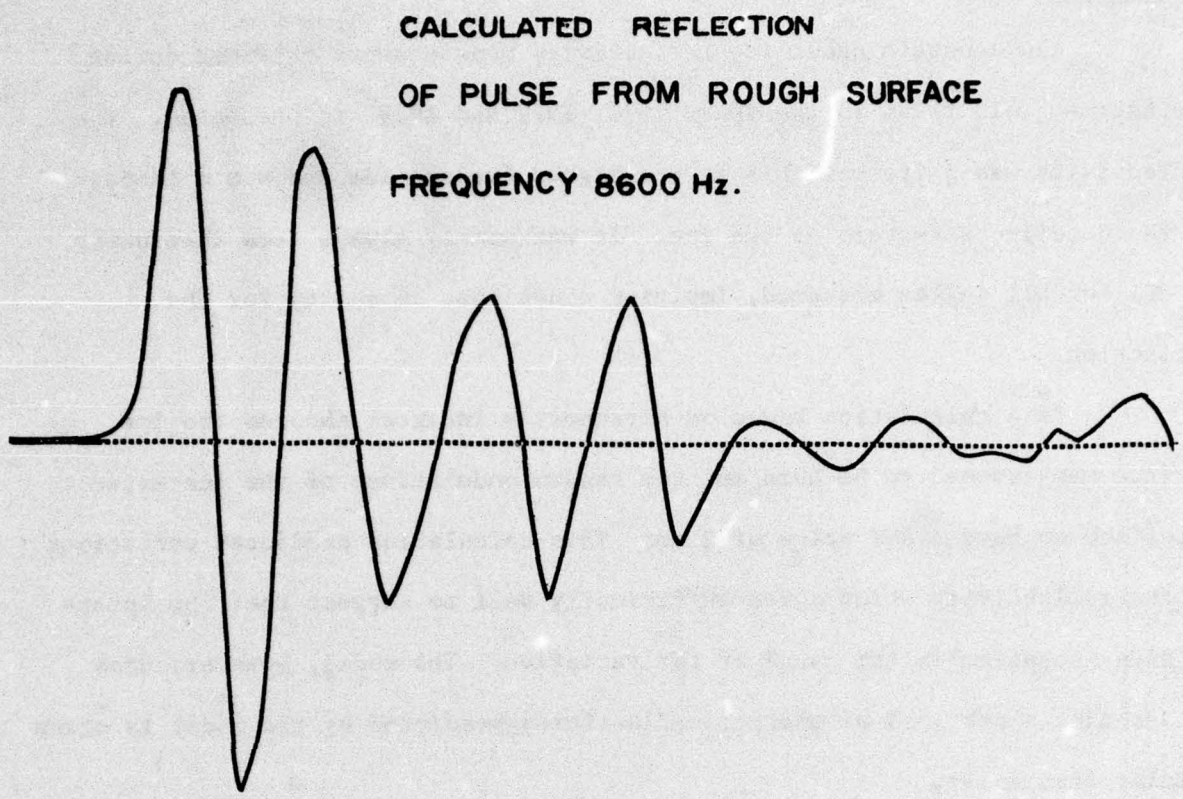

Figure 16. A calculated reflected pulse showing strong interference between successive "Huygen" wavelets.

CONCLUSIONS

The acoustic under-ice reflectivity measurements obtained during springtime field trips in the years 1971, 1972 and 1973 are presented. The reflectivity was quite variable at the higher frequencies and was dependent on the detailed structure of the ice. It was nearly always less than unity (0 dB) for all angles measured, implying a net loss of energy for the reflection.

In a calculation based on Kirchhoff's Integral theorem the ice surface was assumed to be hard and the random undulations of the ice-water interface to have a RMS value of 2 cm. This calculation predicted variations in the reflectivity which agree sufficiently well to suggest that the interference mechanism is the cause of the variation. The model, however, does not predict a net loss of energy; reflectivity predicted by the model is often greater than unity.

REFERENCES

Baker, B. B. and Copson, E. T., 1953, the Mathematical Theory of Huygen's Principle. Clarendon Press.

Born, M. and E. Wolf, 1959, Principles of Optics, Pergammon Press.

Beckermann, P., and Spizzichino A., 1963, the Scattering of Electromagnetic Waves from Rough Surfaces, Pergammon Press.

Eckart, C., 1953, The Scattering of Sound from the Sea Surface, J. Acoust. Soc. Am. 25, 566 - 570.

Ferris, R. H. and Kuperman, W., An Experiment on Acoustic Reflection from the Sea Surface. May 28, 1970, Naval Research Laboratory, Washington, D.C.

Fortuin, L., 1970, Survey of Literature on Reflection and Scattering of Sound Waves at the Sea Surface, J. Acoust. Soc. Am. 47, 1209 - 1228.

Liebermann, L. N., 1948, Reflection of Underwater Sound from the Sea Surface. J. Acoust. Soc. Am. 20, 498 - 503.

Marsh, H. W., 1963, Sound Reflection and Scattering from the Sea Surface. J. Acoust. Soc. Am. 35, 240 - 244.

Marsh, H. W., Schulkin, M. and Kneale, S. G., 1961, Scattering of Underwater Sound by the Sea Surface. J. Acoust. Soc. Am. 33, 334 - 340.

Medwin, H., 1966, Specular Scattering of Underwater Sound from a Wind-Driven Surface, J. Acoust. Soc. Am. 41, 1485 - 1495.

Urick, R. J., 1967, Principles of Underwater Sound for Engineers, McGraw Hill.

APPENDIX A

This appendix derives equations 1 and 2 in the text.

Assuming single frequency acoustic waves, the spatial part of the wave equation reduces to the Helmholtz equation

$$\nabla^2\psi + k^2\psi = 0 \quad \text{where } k = \frac{\omega}{c}$$

Kirchhoff's Integral Theorem (Born and Wolf, 1959; Baker and Copson 1953) states that for a sufficiently well behaved function ψ, the value of ψ at a point P can be expressed as an integral involving the function and its normal derivative evaluated on a surface enclosing the point P.

$$\psi(P) = \frac{1}{4\pi}\iint \left(\frac{e^{iks}}{s}\frac{\partial\psi}{\partial n} - \psi\frac{\partial}{\partial n}\frac{e^{iks}}{s}\right) dS \qquad \text{(A-1)}$$

where s represents the distance from the point P to the surface element and $\frac{\partial}{\partial n}$ represents differentiation with respect to the outward normal.

In application to this report, the enclosing surface consists of the ice-water interface and a hemisphere at infinity. An additional sphere enclosing the source must be included (and integrate over) to exclude the discontinuity at that point from the enclosed region. The integration over this small sphere yields the contribution of the direct arrival and will be ignored in what follows. Also, the integral over the hemisphere at infinity is assumed to be zero. Arguments for this assumption are presented in Born and Wolf (1959). This leaves only the integral over the ice-water interface, and this will yield the amplitude of the reflected wave.

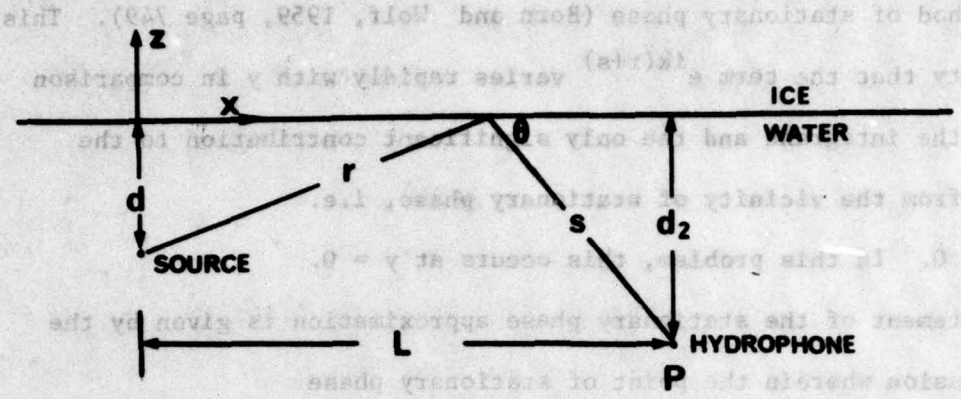

Figure A-1: A schematic diagram illustrating the notation used in the derivation.

With reference to Figure A-1, let r be the distance from the source to the element of area dS and s be the distance from this element to the receiver (point P). We will also assume that the undulations of the ice are gentle enough that the normal derivative is approximately equal to the derivative with respect to z. In the absence of a surface, the value of the incident wave ψ at the element of integration would be $\frac{e^{ikr}}{r}$. The presence of a hard surface causes the value of the function to double and the normal derivative to be equal to zero. Equation A-1 becomes

$$\psi(P) = \frac{1}{4\pi}\iint \frac{-2e^{ikr}}{r} \frac{\partial}{\partial z}\left(\frac{e^{iks}}{s}\right) dxdy$$

$$= \frac{1}{4\pi}\iint \frac{-2e^{ikr}}{r} \frac{e^{iks}}{s}\left(ik - \frac{1}{s}\right) \frac{\partial s}{\partial z}\, dxdy$$

for frequencies where $ks \ll 1$ this reduces to

$$\psi(P) = \frac{-ik}{2\pi}\iint \frac{e^{ik(r+s)}}{rs} \cdot \frac{d_2}{s}\, dxdy \qquad (A\text{-}2)$$

For ease of computation, let us now assume that the surface irregularities are a function of x only, that is $z = z(x)$. We shall integrate over

y using the method of stationary phase (Born and Wolf, 1959, page 749). This uses the property that the term $e^{ik(r+s)}$ varies rapidly with y in comparison to the rest of the integrand and the only significant contribution to the integral comes from the vicinity of stationary phase, i.e. where $\frac{\partial}{\partial y}(r+s) = 0$. In this problem, this occurs at $y = 0$.

A statement of the stationary phase approximation is given by the following expression wherein the point of stationary phase ($h'(y) = 0$) occurs at $y = y_o$.

$$\int_{-\infty}^{\infty} g(y)\, e^{ikh(y)}\, dy = \sqrt{\frac{-2\pi}{kh''(y_o)}}\, e^{\frac{-\pi i}{4}}\, g(y_o)\, e^{ikh(y_o)} \qquad \text{(A-3)}$$

In the present derivation,

$$h(y) = s+r = \sqrt{(L-x)^2+y^2+(d_2+z)^2} + \sqrt{x^2+y^2+(d_1+z)^2}$$

$$h'(y) = 0 \text{ at } y = 0$$

$$h''(o) = \frac{1}{r_o} + \frac{1}{s_o}$$

where $r_o = \sqrt{x^2 + (d_1+z)^2}$ and $s_o = \sqrt{(L-x)^2 + (d_2+z)^2}$

We have, therefore, using equation A-3 to integrate over y,

$$\psi(P) = \sqrt{\frac{k}{2\pi}}\, e^{\frac{-\pi i}{4}}\, d_2 \int_{-\infty}^{\infty} \frac{e^{ik(r_o+s_o)}}{\sqrt{(r_o+s_o)s_o^3 r_o}}\, dx \qquad \text{(A-4)}$$

The lengths r_o and s_o depend on the surface undulation z which must be specified as a function of x in order that the integration may be carried out.

As a check on the equation (A-4) we may evaluate the integral for the case of a flat surface (z = 0). The method of stationary phase is used again, where this time

$$h(x) = s_o + r_o = \sqrt{(L-x)^2 + d_2^2} + \sqrt{x^2 + d_1^2}$$

The condition $h'(x_o) = 0$ occurs at $x_o = \frac{d_1 L}{d_2 + d_1}$ which is the point of geometric reflection. At this point, $h''(x_o) = \sin^2\theta_o \left(\frac{1}{r_{oo}} + \frac{1}{s_{oo}}\right)$ where $\sin\theta_o = \frac{d_1}{r_{oo}} = \frac{d_2}{s_{oo}}$ (see Figure A-1) and r_{oo} is the value of r_o at the point of stationary phase.

Using equation A-3 once more, the approximation yields:

$$\psi(P) = \frac{e^{ik(r_{oo}+s_{oo})}}{r_{oo}+s_{oo}}$$

which, by the method of images, is the expression one would expect for reflection from a hard flat surface.

The expression (A-4) is used to calculate the reflectivities discussed in the text.